Biochimica et Biophysica Acta 1824 (2012) 1016–1023

Contents lists available at SciVerse ScienceDirect

Biochimica et Biophysica Acta

journal homepage: www.elsevier.com/locate/bbapap

Metal binding properties and structure of a type III metallothionein from the metal hyperaccumulator plant *Noccaea caerulescens*

Lucia Rubio Fernandez [a,1], Guy Vandenbussche [b], Nancy Roosens [a,2], Cédric Govaerts [b], Erik Goormaghtigh [b,*], Nathalie Verbruggen [a]

[a] Laboratoire de Physiologie et de Génétique Moléculaire des Plantes, Université Libre de Bruxelles (ULB), B-1050 Brussels, Belgium
[b] Laboratory for the Structure and Function of Biological Membranes, Center for Structural Biology and Bioinformatics, ULB, Brussels, Belgium

ARTICLE INFO

Article history:
Received 24 January 2012
Received in revised form 7 May 2012
Accepted 25 May 2012
Available online 2 June 2012

Keywords:
Metallothionein
Heavy metal
Plant
IR spectroscopy
Metal binding
Mass spectrometry

ABSTRACT

Metallothioneins (MT) are low molecular weight proteins with cysteine-rich sequences that bind heavy metals with remarkably high affinities. Plant MTs differ from animal ones by a peculiar amino acid sequence organization consisting of two short Cys-rich terminal domains (containing from 4 to 8 Cys each) linked by a Cys free region of about 30 residues. In contrast with the current knowledge on the 3D structure of animal MTs, there is a striking lack of structural data on plant MTs. We have expressed and purified a type III MT from *Noccaea caerulescens* (previously *Thlaspi caerulescens*). This protein is able to bind a variety of cations including Cd^{2+}, Cu^{2+}, Zn^{2+} and Pb^{2+}, with different stoichiometries as shown by mass spectrometry. The protein displays a complete absence of periodic secondary structures as measured by far-UV circular dichroism, infrared spectroscopy and hydrogen/deuterium exchange kinetics. When attached onto a BIA-ATR biosensor, no significant structural change was observed upon removing the metal ions.

1. Introduction

In heavy metal polluted soils a class of rare plants, called hyperaccumulators, are able to accumulate exceptional high concentrations of trace elements in their aerial parts without visible toxicity symptoms (reviewed in [1,2]). Cd is one of the most toxic metals for living organisms and *Noccaea* (previously named *Thlaspi caerulescens*) is one of the four identified Cd hyperaccumulators identified up to now [1–4]. Its relatedness to the model species *Arabidopsis thaliana* microarrays has allowed molecular insights on hyperaccumulation mechanisms through the use of *Arabidopsis* DNA chips (reviewed in [1,2]). Comparative global transcriptomics studies have shown that as part of resistance to high metal concentration a large array of genes are constitutively (in the absence of metallic ions excess) highly expressed in *Noccaea caerulescens* compared to *Arabidopsis* or other non-hyperaccumulator closely related species [5–7]. Among many other groups of genes (the main category being metal transporters, [5–7]), those coding for metallothioneins (MTs) are highly overexpressed [4].

Since their discovery in horse kidney [8], MTs have been found in nearly all living organisms, although showing a high heterogeneity of sequence. MT superfamily is defined as comprising all polypeptides which resemble equine renal metallothionein in several of their features such as low molecular weight (<10 kDa), high metal content, low content of aromatic amino acids, amino acid sequence with motifs containing numerous Cys with a characteristic distribution, and spectroscopic manifestations typical of metal thiolate clusters [9,10]. Based on sequence similarities and phylogenetic relationships, plant MTs have all been regrouped in family #15 which differs from animal ones by a peculiar amino acid sequence organization consisting generally of two short Cys- rich terminal domains linked by a spacer region without Cys. The length of this region and the distribution of the Cys residues are the basis of further classification of plant MTs into three types. There is a separate subfamily, named plant Ec proteins or MT4 proteins, differing from other plant MTs by having three Cys-rich domains separated by 10 to 15 residues [9,10].

In contrast with the current knowledge on the 3D structure of animal MTs [11–13] there is a lack of structural and functional data on the plant MT isoforms. Ec-1 is the first and so far only plant MT for which the 3D structure of N- and C-domains has been determined [14,15]. Native MT proteins were found to be difficult to isolate

Abbreviations: IR, infrared; FTIR, Fourier Transform infrared; ATR, attenuated total reflection; CD, circular dichroism; MT, metallothionein

* Corresponding author at: Center for Structural Biology and Bioinformatics, Laboratory for the Structure and Function of Biological Membranes,Campus Plaine CP206/02; Université Libre de Bruxelles, Bld du Triomphe 2, CP206/2, B1050 Brussels, Belgium. Tel.: +32 2 650 53 86; fax: +32 2 650 53 82.
E-mail address: egoor@ulb.ac.be (E. Goormaghtigh).
[1] Structural Biology Brussels, Vrije Universiteit Brussel, Pleinlaan 2, B-1050 Brussels, Belgium and Department of Structural Biology, VIB, Pleinlaan 2, B-1050 Brussels, Belgium.
[2] Scientific Institute of Public Health Avenue Juliette Wytmans 14 1050 Brussels, Belgium.

1570-9639/$ – see front matter © 2012 Elsevier B.V. All rights reserved.
doi:10.1016/j.bbapap.2012.05.010

from plants but recombinant DNA technology provides new insight into the biochemical characterization of plant MTs.

A general structure for plant MT has been proposed for *Triticum durum* MT type I. This protein forms dimers or higher oligomers and adopts an extended conformation containing both α-helix and β-sheet structures. This model proposes an overall dumbbell shape similar to that reported for mammalian MTs [16], in agreement with dynamic data obtained on *Fucus vesiculosus* MT [17]. *Quercus suber* MT type II adopts a mainly β-sheet structure (60% of the sequence) with no α-helix as evaluated from circular dichroism, Raman and infrared spectra [18,19]. The involvement of peptide donor groups (S-thiol and N-imidazole) and non-protein ligands (as sulfide anions) in metal chelation, as well as secondary structure elements, was demonstrated. The protein accommodates up to six Cd^{2+} together with four S^{2-} while less than four Zn^{2+} could bind the protein. Interestingly, the fraction of β-sheet in the protein significantly increased in the presence of Cd^{2+}. Wheat (*Triticum aestivum*) E_c-1 MT displays two distinct metal thiolate clusters [20].

Here, we expressed, purified and characterized NcMT3, a MT type III from *N. caerulescens*, which was previously isolated in a screen for Cd tolerance in yeast [4,21]. The structural properties of the protein were characterized using far-UV circular dichroism, infrared spectroscopy and hydrogen/deuterium exchange kinetics. Mass spectrometry measurements revealed the presence of cations that bind to NcMT3. The physiological relevance of these findings is discussed.

2. Materials and methods

2.1. Production and purification of recombinant NcMT3

2.1.1. Construction of plasmid

The MT3 sequence of *N. caerulescens* cDNA (GenBank: AY531114.1 ; GI:46487744) was cloned into *Escherichia coli* Rosetta strain (F^- *ompT* *hsdS*$_B$(r_B^- m_B^-) *gal dcm* pRARE (Cam^R)) in the vector pTWIN2 from the IMPACT™-TWIN system (New England Biolabs) using the *XhoI* and *EagI* restriction sites. The accuracy of the insert and the integrity of the sequence of the plasmid were confirmed by DNA sequencing.

2.1.2. Protein overexpression and purification

N. caerulescens MT3 was overexpressed in *E. coli* Rosetta strain as a fusion protein with a vector-derived N-terminal intein tag (protein self-splicing element) and a chitin-binding domain under the control of T7 promoter according to procedures described in the IMPACT™-TWIN manual.

E. coli cells were grown in 1.5 concentrated LB broth, induced with IPTG for 4 h, harvested by centrifugation and resuspended in washing buffer (100 mM NaCl, 0.5 mM phenylmethylsulphonyl fluoride (PMSF) and 20 mM Hepes, pH 7.0). Pellets were stored at −80 °C for further use.

As the *NcMT3* cDNA used in this study was cloned from a population of *N. caerulescens* (Les Malines) which grows in soils highly polluted with Pb, Zn and Cd [4,22], the protein was purified in presence of either one of these three ions, as well as Cu^+, due to the reported MT role in copper homeostasis [4]. Mn was chosen as control metal, due to its role as essential trace nutrient.

Cells from an 8 L bacteria culture were resuspended in 200 mL buffer (20 mM HEPES, pH 8.5, 50 mM NaCl, 0.1 μL/mL PMSF and 2 μL/mL β-mercaptoethanol) and lysed by homogeneization and with Emulsiflex (Avestin). After centrifugation, the supernatant was applied to a chitin column (New England Biolabs) equilibrated with buffer containing 500 mM NaCl, 20 mM Hepes, pH 8.5 and one of each metal 1) 250 μM $CdSO_4$, 2) 250 μM $ZnSO_4$, 3) 250 μM $Pb(CH_3COO)_2$, 4) 250 μM $MnSO_4$ or 5) 250 μM $CuSO_4$, adding in this case 1.25 mM of ascorbic acid to obtain Cu (I). Following extensive washing with increasing salt concentrations (up to 500 mM NaCl), on-column self-cleavage of the intein tag was induced with 50 mM NaCl, 20 mM HEPES, pH 7.0, 250 μM of tested metals, 0.01 mM PMSF and 2 μL/mL β-mercaptoethanol overnight at 4 °C.

Crude NcMT3 elute was concentrated up to 500 μL prior to a final purification step with size-exclusion chromatography using a Superdex 75/300 GL column (GE Healthcare) and a buffer containing 150 mM NaCl, 20 mM Hepes and 10 mM β-mercaptoethanol, pH 7.0. NcMT3 protein eluted in a single peak was again concentrated to 500 μL for samples purified in the presence of Cu^+, Zn^{2+}, Cd^{2+} and 250 μL for those with Mn^{2+} and Pb^{2+}, and was used directly for infrared and CD assays or was stored at – 80 °C before ESIMS assays.

2.2. Mass spectrometry

Molecular mass determination: Prior to mass spectrometry analysis, the buffer of protein samples was exchanged to 10 mM ammonium acetate, pH 6.9 using Amicon Ultra-4 centrifugal filter unit (3,000 NMWL, Millipore, Billerica, USA). The protein solutions were loaded into gold-palladium coated borosilicate nanoelectrospray capillaries (Proxeon, Odense, Denmark). The mass spectra were acquired on a Q-Tof Ultima mass spectrometer (Waters/Micromass, Milford, USA), equipped with a Z-spray nanoelectrospray source and operating in the positive ion mode. Capillary voltages of 1.8–2.0 kV and cone voltage of 50 V typically were used. The source temperature was held at 100 °C. The time-of-flight analyzer was operated in the V mode. The molecular masses were determined after Maximum Entropy processing of the raw spectra (MaxEnt1 — Waters/Micromass, Milford, USA).

2.2.1. Protein microsequencing

Digestion of the protein was performed by enzymatic proteolysis or by microwave-assisted acid hydrolysis [23]. In the first case, the Cys residues of NcMT3 were alkylated with 40 mM iodoacetamide after reduction in the presence of 10 mM DTT. The digestion was realized overnight at 37 °C in the presence of sequencing grade modified trypsin (Promega, Madison, USA). In the second case, the protein was solubilized in 25% TFA (v/v), 20 mM DTT and was irradiated during 10 min in a domestic 750 W microwave oven. The peptides generated by enzymatic or chemical digestion were solubilized in 0.5% TFA (v/v), desalted on $ZipTip_{C18}$ (Millipore, Billerica, USA) and eluted in 50% acetonitrile/1% formic acid (v/v) prior to analysis by tandem mass spectrometry (MS/MS).

2.3. FTIR and CD spectroscopies

FTIR spectroscopy was used in this study because it allows the monitoring of the secondary structure of μg quantity of protein in different environments (different metals) and also the recording of H/D exchange kinetics.

2.3.1. Acquisition of ATR-FTIR spectra

Attenuated total reflection infrared (ATR-FTIR) spectra were obtained on a Bruker IFS55 FTIR spectrophotometer (Ettlingen, Germany) equipped with a MCT detector (broad band 12000–420 cm^{-1}, liquid N_2 cooled, 24 h hold time) at a resolution of 2 cm^{-1} with an aperture of 3.5 mm and acquired in double-sided, forward-backward mode. The spectrometer was purged with dry air. The internal reflection element was a 52×20×2 mm trapezoidal germanium ATR plate (ACM, Villiers St Frédéric, France) with an aperture angle of 45° yielding 25 internal reflections. The germanium crystals were washed and thin films formed as described [24,25].

After recording, a baseline subtraction and correction for atmospheric water absorbance were carried out as previously [26].

2.3.2. $^1H/^2H$ exchange kinetics

For hydrogen/deuterium exchange, nitrogen gas was saturated with ^2H_2O by bubbling through a series of four vials containing ^2H_2O at a flow rate of 50 mL/min controlled by a flowtube (Fisher Bioblock Scientific, Illkirch, France) as described previously [27,28].

The area of the lipid ν(C═O), amide I, II and II′ were obtained by automatic integration. For each spectrum, the area of amide II was divided by the area of amide I in order to take into account the swelling of the sample layer due to the presence of ^2H_2O [25,29].

2.3.3. Flow experiments

Triangular-shaped germanium crystals ($4.8\times4.8\times45\ mm^3$) were purchased from Biosentech (Naninne, Belgium) and accommodated on the beam condenser from a Golden Gate Micro-ATR from Specac. A top plate with a groove fitting the crystal was used in replacement of the diamond-bearing plate (WOW Company, Belgium). With this geometry, a single reflection occurs and more than 10 lanes can be used on a crystal. Covalent grafting was carried out as previously described for the BIA-ATR technology [30,31] were carried out sequentially as described in [30]. In final photografting of O-succinimidyl 4-(*p*-azidophenyl)butanoate yielded an activated ATR element ready for covalent fixation of proteins.

All the infrared spectra and further analyses were processed by the software "Kinetics" generated in our lab and running under MatLab (Mathworks Inc, Natick, MA).

2.3.4. CD data collection and processing

To confirm FTIR structural data (far UV) and get more information about the folding of the protein (near UV), CD was used. CD spectra were collected on a JASCO J-710 CD spectrometer using protein solutions in 2 mM HEPES pH 7.2 in the presence of the different metal ions in a 0.1 cm cell. Each CD spectrum was the accumulation of 8 scans at 50 nm/min with a 1 nm slit width and a time constant of 0.5 s for a nominal resolution of 1.7 nm. Data were collected from 185 to 260 nm [32,33] for far UV CD and from 260 to 320 nm for near UV-CD. In the latter case the concentration was 10 times higher.

3. Results

3.1. Characterization of purified NcMT3 from N. caerulescens

NcMT3 was expressed in *E. coli* as a fusion with a N-terminal intein tag within the IMPACT™ system (New England Biolabs) and purified on a chitin column in the presence of metal ions. After pH-induced cleavage, an additional gel filtration purification step was performed. The protein could be isolated from a single peak on size-exclusion chromatography which, upon re-injection remained as a single Gaussian peak at the same elution volume (Fig. 1). Purification using the different metal ions showed identical behaviors on gel filtration albeit with different yield (not shown) while it was impossible to obtain the apoprotein purifying NcMT3 in complete absence of heavy metals, since the chromatogram showed a denaturated protein (not shown). On a Superdex 75/300GL size exclusion column NcMT3 elutes at 13 mL which, according to parallel runs with protein standards, fits an apparent mass of 17 kDa, which could correspond to a dimer. Yet, the apparent mass could also reflect a non-globular shape of the protein. The apparent mass appears fully stable in solution as it is maintained upon re-injection.

In order to obtain the apoprotein, NcMT3 was initially purified in the presence of Cd^{2+} and subsequently incubated with EDTA or at low pH as described in [34]. Incubation with EDTA led to apparent aggregation of the protein while low pH allowed recovery of apoMT3 as shown by mass spectrometry (data not shown). However, the protein was not able to bind metal after low pH treatment, indicating a probable denaturation.

Quantification of the recombinant NcMT3 protein has proven difficult, as the absence of Trp or the presence of only two Tyr prevents absorbance measurements at 280 nm while the use of chromatic dyes (i.e. Bradford method) was hindered due to the absence of Arg residues

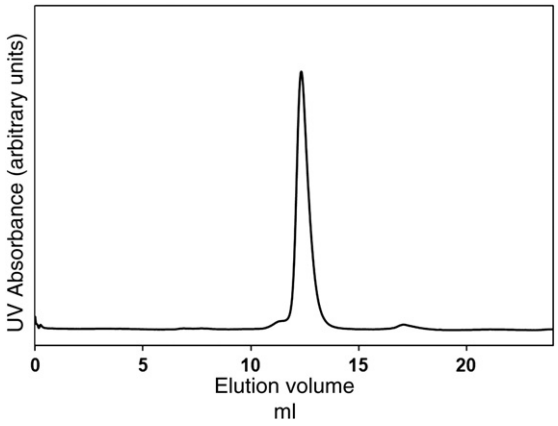

Fig. 1. Size exclusion profile (recorded at 280 nm) of the recombinant NcMT3 purified in the presence of Cd^{2+}. This profile corresponds to the reinjection of the NcMT3 peak coming from the size-exclusion chromatography of the chitin-column elution. The purified peak maintains a single peak morphology eluting at 13 mL.

3.2. Metal binding by mass spectrometry

The molecular mass of the recombinant NcMT3 was determined by mass spectrometry. In the presence of 10 mM β-mercaptoethanol and after desalting on $ZipTip_{C18}$ (Millipore, Billerica, USA) at low pH, the apoprotein shows an experimental mass of 7620.2 Da (Fig. 2), value that is not in agreement with the expected theoretical mass. The sequence of the protein was therefore controlled by microsequencing by mass spectrometry. The protein was digested in the presence of trypsin or by microwave-assisted acid hydrolysis [23]. This latter approach was chosen for its propensity to enrich the peptide mixture in N- and C-terminal fragments. Analysis of the tryptic peptides and of the acid hydrolysis products allowed the detection of five additional N-terminal residues in comparison with the NcMT3 sequence (Fig. 3). These extra vector derived residues lead to a protein with a theoretical mass of 7620.677 Da in good agreement with the measured mass.

The recombinant NcMT3 purified in the presence of different heavy metal ions was analyzed by ESI-MS in 10 mM ammonium acetate at pH 6.9. In the presence of Cd, the mass spectrum revealed the presence of three metalloforms with metal stoichiometries of 3, 4 and 5 (Fig. 4A). When the protein was purified in the presence of Zn, the forms presented a metal stoichiometry of 4, or 5 (Fig. 4B). The profile

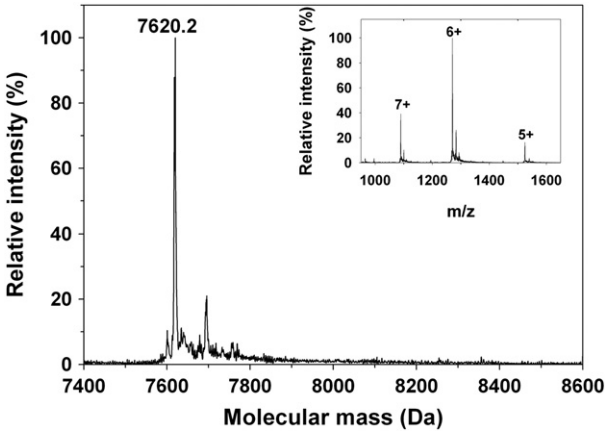

Fig. 2. Deconvoluted ESI-MS spectrum of the recombinant apoNcMT3. The inset represents the m/z spectrum in the range 1000–1700 with the charge-states indicated. The protein incubated in the presence of 10 mM β-mercaptoethanol was desalted on $ZipTip_{C18}$.

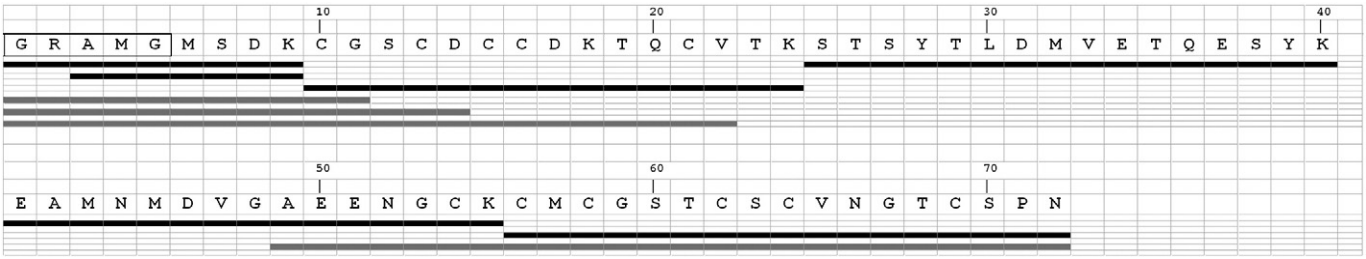

Fig. 3. Sequence of the recombinant NcMT3 determined by microsequencing. The sequenced peptides obtained after trypsin digestion or acid hydrolysis are represented by the black and gray lines, respectively. The additional five N-terminal residues are in a box.

was very similar in the presence of Pb even if in this case, a very small peak associated with a putative population containing six equivalents of Pb^{2+} was observed (data not shown). In the case of Cu(I), no specific interaction could be detected (data not shown). The recombinant NcMT3 had a lower affinity for Mn as only one metal ion was associated with the protein (data not shown). In addition, the apoform of the protein was still observed in the spectrum which was not the case with the other metal ions tested in this study.

3.3. Secondary structure of MT3: FTIR and CD spectroscopies

3.3.1. FTIR spectra of NcMT3

ATR-FTIR spectra of NcMT3 purified in the presence of Cu^{+}, Pb^{2+}, Zn^{2+}, Mn^{2+} and Cd^{2+} ions are presented in Fig. 5, panel A. The bands around 1650 cm^{-1} (Amide I) and 1535 cm^{-1} (Amide II) arise mainly from the absorption of proteins. Amide I is the most intense absorption band of the polypeptides. It is positioned between 1700 and 1600 cm^{-1}, but its exact frequency is determined by the geometry of the polypeptide chain and hydrogen bonding. The vibration of the main chain carboxyl group ν(C═O) has a predominant role in amide I accounting for 70–85% of the potential energy, while ν(C–N) follows with 10–20% of the potential energy and the C–CN deformation may account for about 10% of the potential energy [35]. The band at 1535 cm^{-1} is the amide II contribution (typically observed in the 1510–1580 cm^{-1} region). It derives mainly from the in plane N–H bending (40–60% of the potential energy). The rest of the potential energy arises from ν(C–N) (18–40%) and ν(C–C) (~10%) [35]. The shoulder at 1517 cm^{-1} is assigned to the Tyr ring.

The presence of amide I at 1651 cm^{-1} could indicate a high proportion of α-helix in the protein. Yet, the position of amide II at 1535 is not compatible with that possibility as α-helices are known to absorb near 1545 cm^{-1} in the amide II [36,37], indicating that the dominant structure could rather be random. Because of the particularly high proportion of acidic amino acid residues (10 residues on a total of 70), and as these residues absorb in the amide I–amide

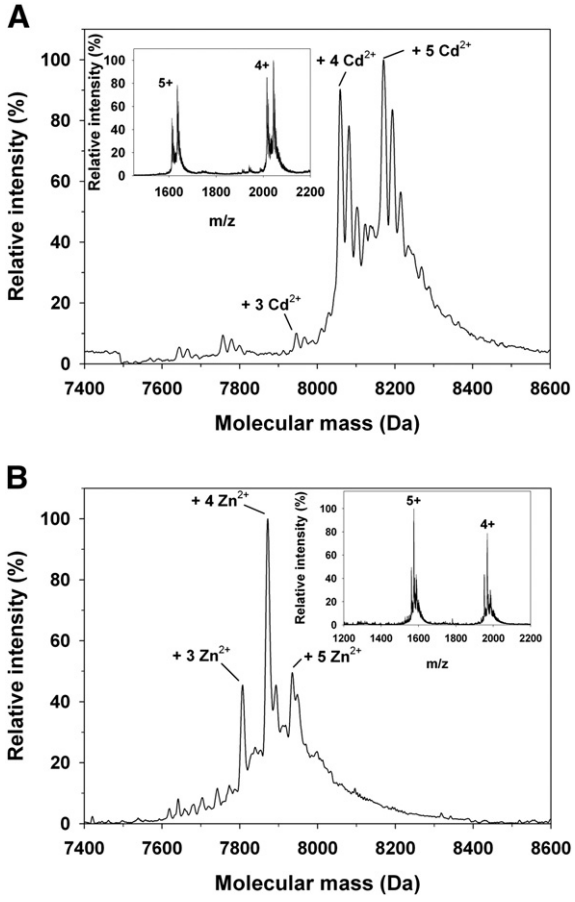

Fig. 4. Deconvoluted ESI-MS spectra of the recombinant NcMT3 purified in the presence of 250 μM Cd^{2+} (A) or 250 μM Zn^{2+} (B). The number of metal ions associated with the different protein populations is indicated. The inset represents the m/z spectra with the charge-states indicated.

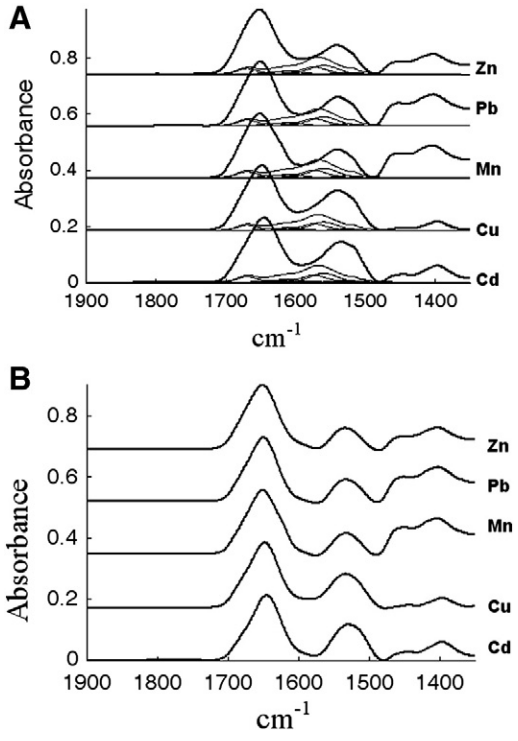

Fig. 5. ATR-FTIR spectra of NcMT3 in the presence of different metal ions (Zn^{2+}, Pb^{2+}, Mn^{2+}, Cu^{+}, Cd^{2+}) in the 1900–1300 cm^{-1} region of the spectrum. For a better reading, the spectra have been offset by 0.14 absorbance units. A. Original spectra with the contributions of the lateral side chains in the amide I–amide II range. The individual contributions from the side chains as well as their sum are plotted under every spectrum. B. Spectra of part A of the figure corrected for the amino acid side chain contribution.

II range, the side chain contribution was computed, scaled and subtracted as summarized in [37,38] . The spectra corrected for the side chain contribution are presented in Fig. 5, panel B. Amide I still appears at 1651 cm^{-1} as a rather homogenous band but also as a rather broad (full width at half height (FWHH) = 58 cm^{-1}), further suggesting the presence of random conformation as the major structure. Indeed, α-helices are characterized by FWHH close to 30 cm^{-1} while random conformation are found to have FWHH ranging from 55 to 65 cm^{-1} [37,39].

An analysis of the secondary structure was carried out as described in [39,40]. Results are reported in Table 1. This analysis is in agreement with a largely disordered protein. In another attempt we compared the spectrum of NcMT3 with an ATR-FTIR protein spectra present in a FTIR database [41] optimized to cover as well as possible the different structural folds as described by CATH and SCOP [41,42]. A hierarchical clustering (not shown) indicated that the closest spectrum in the entire database was the spectrum of a rabbit metallothionein II (Swiss-Prot MT2A_RABIT, PDB 4mt2) introduced into the database to represent a fully unstructured protein.

3.3.2. CD spectra of NcMT3

Representative far UV CD spectra are presented in Fig. 6. Because of the difficulty to obtain exact protein concentration, no attempt was made to obtain the secondary structure content from these CD spectra. Yet, it is obvious that the spectra presented have a shape that is characteristic of random structure and not of helical structure. Indeed, helical structures have a double minimum at 208 and 222 nm that is completely absent. β-Sheet structures have a less intense minimum at 225 nm which is also absent here. On the other hand, the random structure has a distinct minimum around 200 nm in good agreement with the spectra of NcMT3 observed here.

Near UV-CD spectra of NcMT3 complexed with Zn^{2+} and Pb^{2+} appear in Fig. 7. It has been reported for a type II MT from *Q. suber* [43] that complexes with Cd^{2+} but not Zn^{2+} display two main positive bands in the near-UV CD spectrum at 250 nm related to the involvement of His and 275 nm indicating the participation of sulfide ligands in the Cd-MT complex. Such maxima do not appear here suggesting a different mechanism of metal binding. Near UV-CD spectra of a number of metal binding configurations have been obtained for animal MT [44]. None of them corresponds exactly to the data obtained here.

Overall, ATR-FTIR and CD spectra strongly indicate that the different metal-bound protein species adopt a largely random structure.

3.3.3. Flow experiments

NcMT3 was covalently attached to a germanium internal reflection element as described in Methods and the sample was placed in a sealed chamber with an in- and outlet. ATR-FTIR spectra were recorded as a buffer was flowing over the grafted NcMT3 molecules. The buffer flow composition was designed to remove or add the metal cations. With such an experimental design, protein conformational changes could be monitored on-line as the buffer composition is manipulated [45]. In similar experiments, conformational changes induced by replacing Na^+ ions by K^+ ions in a H^+,K^+-ATPase were demonstrated to change the secondary structure of 2% of the protein [46]. In order to attach NcMT3 covalently to the germanium surface, a polyethylene glycol (PEG) layer was first attached by silanization to prevent unspecific protein adsorption and denaturation on the surface [30]. An activated ester was then photografted on the PEG molecules to provide an attachment group for the primary amino groups (N terminal or ε-NH_2 of lysines) of proteins [30]. Cd-MT3 was finally incubated in the presence of the activated/grafted germanium surface of the sensor for 3 h according to the established protocol. Attachment of the protein could be monitored by the growing intensity of the amide I and amide II bands of the protein as it was binding on the germanium surface where the evanescent wave has the largest intensity (not shown). Amide I appears as a broad band centered around 1651 cm^{-1}, confirming that the protein random structure was not modified upon binding. Binding was stable under rinsing with buffer. In a second step, the cell was flushed with the buffer alone containing EDTA (1 mM). Simultaneously, ATR-FTIR spectra of the protein were recorded in order to observe potential structural changes induced by removal of the cations. No significant structural modification of the protein could be detected (data not shown). In other experiments (not shown), the metal was reintroduced in the buffer flowing in the biosensors after removal of EDTA. Again, no significant change could be observed in the IR spectrum of NcMT3.

Table 1
Evaluation of the secondary structure content in NcMT3 by analysis of the ATR-FTIR spectra. The analysis has been carried out as described in [40] and is not constrained to 100%.

α Helix:	4%
β Sheet:	11%
Random	55%
β Turns	3%

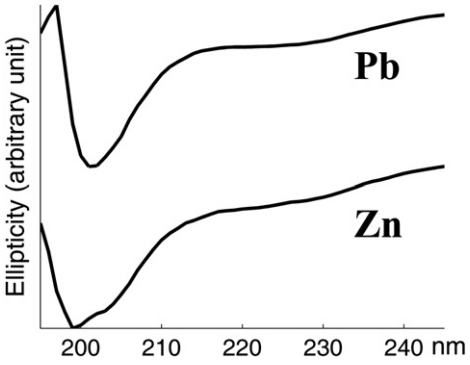

Fig. 6. Far-UV circular dichroism spectra of NcMT3 in the presence of metal cations Pb and Zn. For a better readability, spectra have been offset.

3.3.4. $^1H/^2H$ exchange kinetics

Hydrogen isotope exchange has long been used for the analysis of protein structure and dynamics [47–50]. It appears to be one of the main techniques capable of identifying submolecular motional domains including fast exchanging protons of the protein surface, somewhat slower exchanging protons of the flexible (loop) regions buried in the protein or involved in some secondary structures and the slowly exchanging protons from the protein core formed by the most rigid clusters (knots) of amino acids. $^1H/^2H$ exchange allows the characterization of the protein stability in different experimental conditions.

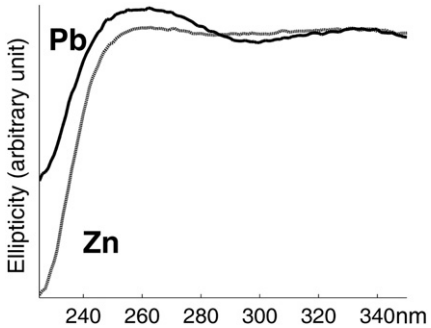

Fig. 7. Near-UV circular dichroism spectra of NcMT3 in the presence of metal cations indicated on the figure.

Conformational changes relevant to an enzyme catalytic cycle could be identified for different proteins by FTIR spectroscopy [25,46,51–53].

A series of IR spectra showing the progression of the $^{1}H/^{2}H$ exchange are shown in Fig. 8 for a representative kinetics recorded in the presence of Zn^{2+}. As expected, few changes are detected in the 1700–1600 cm^{-1} region upon $^{1}H/^{2}H$ exchange, whereas the intensity of amide II band decays concomitantly with an increase in amide II intensity at 1500–1400 cm^{-1}. To better follow the disappearance of amide II band, its area was calculated and plotted against deuteration time (not shown). The evolution of amide II band as a function of time of exposure to $^{2}H_2O$ (Fig. 8) demonstrates that the exchange is extremely rapid with basically only one intermediate (15 s) between the first 10 spectra recorded before the beginning of the deuteration and the rest of the experiment (i.e. between 30 s and 6 h). After 30 s deuteration, the amide II is present as a tilted flat line between 1570 and 1500 cm^{-1} indicating that the protein reached full deuteration within the first 30 s. The band rising at 1570 cm^{-1} is due to the Asp and Glu side chains whose intensity increased during the hydration of the protein by $^{2}H_2O$. Tyr side chain contribution is visible as a narrow peak at 1515 cm^{-1} [54,55]. Similar exchange measurements were repeated in the presence of Pb^{2+}, Cu^{+}, Mn^{2+} and Cd^{2+}. All were characterized by similar fast exchange rates.

Such a rapid exchange is not observed for most structured proteins whose exchange span a period of several hours to several days [56–60]. It confirms the absence of secondary structure in NcMT3 in the presence of the different cations tested.

4. Discussion

4.1. Cation specificity of NcMT3

Up to five Cd^{2+} metal ions can bind to NcMT3. When purified in the presence of Zn^{2+}, the protein was able to bind 4 and 5 Zn^{2+}.

In the plant MT3 subfamily which usually counts 10 cys residues, the calculated range is 3,3-4,6 metal ions (10). Here NcMT3 contains 11 cys and coordination of 4 to 5 divalent ions is well within the predicted range. In other MT3, 4 Cd^{2+}, 3 to 4 Zn^{2+} were determined for *Musa acuminata* (banana) [61] and only 1,7 Zn^{2+} for *Elaeis guineensis* (oil palm) MT3a [62].

In comparison *Q. suber* MT2 [19] also binds 5 Zn^{2+} but wheat Ec1 , containing 17 Cys residues, are able to bind 6 Zn ions [10,20] . Binding of Pb^{2+} to plant MT was already reported for banana MT3 [61], but some mammalian metallothionein can bind up to 7 Pb^{2+} [63,64]; 4 to 6 Pb^{2+} ions could bind to the recombinant NcMT3. Those results combined with the fact that NcMT3 gene used in this study was cloned from a *N. caerulescens* population which grows in soils highly polluted with Pb, Zn and Cd, suggest that NcMT3 could be involved in Cd and Pb detoxification and to a lesser extent Zn. In strong support, heterologous expression of *NcMT3* in *Saccharomyces cerevisiae* protected cells against Cd and Cu toxicity and to a lesser extent to Zn excess [4].

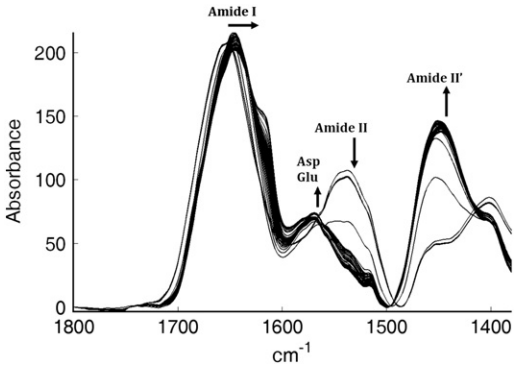

Fig. 8. Series of ATR-ATR spectra recorded as a function of time in the presence of a $^{2}H_2O$-saturated N_2 flow.

It is important to note that mass spectrometry indicates that no S^{2-} ions were present in the preparation, suggesting that the 11 Cys residues present are sufficient to bind metal ions while in some plant and animal MT several additional S^{2-} ions are thought to participate in the binding. For instance *Q. suber* MT type 2 accommodates up to 6 Cd^{2+} with the participation of 4 S^{2-} [18]. Furthermore, as no His are present in the protein, it is likely that binding occurs only through interaction with the 11 Cys In banana and oil palm MT3, an additional His residue is thought to serve as ligand [61], in the wheat EC1 two histidine residues participate in metal binding [65].

Interestingly, Hassinen et al. [66] found differences in MT3 gene sequences in various *N. caerulescens* populations from different areas and soil metal ion content. Expression levels were different for the different proteins but with no correlation with Zn accumulation capacity. The results suggested that the differential MT expression observed among the accessions was not a directly related to variation in Zn accumulation capacity. The present protein did bind Zn in vitro, suggesting that a further evaluation of its function with respect to Zn should be considered.

4.2. Structural characterization of NcMT3

A survey of the available three-dimensional structures of animal metallothioneins shows that, while adopting a variety of folds, they present a common architecture. MTs present little or no secondary structures but, however, are rigidly structured. The driving force for such structure is metal ion coordination through Cys, which imposes the overall fold.

In the case of plant MTs the situation might be more complex. Beside the wheat E_c-1 [14,15], no three-dimensional structure is available on plant MTs. As recently reviewed [10] sequence analysis of some plant MT1, MT2, MT3 and E_c-1 reveal that no -helix is expected but -sheet is predicted to form ca 30% of the structure content. Experimentally, the wheat E_c-1 MT was found to be devoid of regular secondary structure and shows a typical metal-induced structure [20]. On the basis of Raman and infrared spectroscopy data obtained in the presence of metal it was proposed that *Q. suber* MT2 would adopt a mainly β-sheet structure (60% of the sequence) with no α-helix [19]. *Cicer arietinum* MT1 was also shown to contain ca 30% -sheet by infrared spectroscopy and circular dichroism [67]. A preliminary report on a MT3 (in [10]) also suggests the presence of ca 30% -sheet in this protein.

The secondary structure of NcMT3 was investigated here by FTIR and CD spectroscopy as well as by hydrogen/deuterium exchange kinetic measurements. Both CD and FTIR lead to the conclusion that little or no periodic (α-helix, β-sheet) structure was present in NcMT3. It must be stressed that the absence of regular periodic secondary structure (α-helix, β-sheet) for all the metals tested does not preclude the presence of a particular tertiary fold for the protein. While α-helices and β-sheets have characteristic shapes in the FTIR and CD spectrum [33,40,41,68,69], the so-called random/coil structure is a complex mixture of peptide bond conformations which contributes in all parts of the amide I region, overlapping the contributions of the periodic secondary structures. Similarly, β-turns are characterized by a large variety of conformations whose analysis remains difficult. The extremely rapid H/D exchange observed for NcMT3 shows that backbone hydrogens are particularly exposed to the solvent, which is consistent with the typical MT architecture. Data obtained here support that NcMT3 structure is distinct from the few plant MT described up to now, and that it behaves like some animal MT, adopting a non periodic – but not unfolded – structure. Finally, when compared to a database containing the infrared spectra of proteins selected to cover the conformational space as well as possible [40,41], a cluster analysis shows that the closest neighbor of NcMT3 in the whole database is

the MT2A metallothionein from rabbit liver (data not shown). This protein has no periodic secondary structure.

At this point it is important to question the validity of the structure of this purified, heterologously expressed, protein. Over-expression of this plant protein in bacteria could potentially result in a misfolded protein. Even though it cannot be definitively demonstrated that he protein is in its native structure, metal binding experiments indicate that this function is retained with variations from one metal to another commonly encountered in MTs. When EDTA is added to NcMT3 in solution, the protein precipitates. In agreement with this behavior in solutions, size exclusion chromatography reveals that NcMT3 cannot be purified in the absence of any metal (not shown). When attached to the polyethylene glycol surface of a BIA-ATR biosensor, the behavior appears to be quite different as no structure change could be observed, even though infrared spectroscopy is very sensitive to protein aggregation. This result suggests that:

- ApoNcMT3 is stable in the environment present at the biosensor surface. This specific environment crowded with protein molecules and polyethylene glycol chains could be in fact more representative of the intracellular conditions.
- No significant structural change occurs upon releasing the metal ion, suggesting in turn that minor movement of hinge regions are sufficient to drive the key residues to the position favorable to bind the metal, i.e. the tertiary folding might change to allow proper interactions between Cys residues and the metal but this does not involve formation of new secondary structures.

In conclusion, the present report suggests that NcMT3 is mainly devoid of periodic secondary structure, a new feature in plant MT1, MT2 and MT3 families.

Acknowledgement

EG is Director of Research and CG Research Associate with the Fonds National de la Recherche Scientifique (FNRS, Belgium) and L.R was FNRS PhD student. This work was supported by the Belgian Science Policy (Interuniversity Attraction Pole Programme VI/33), and the FNRS (Fonds de la Recherche Fondamentale Collective grants 2.4.558.08 and 2.4527.10).

References

[1] N. Verbruggen, C. Hermans, H. Schat, Molecular mechanisms of metal hyperaccumulation in plants, New Phytol. 181 (2009) 759–776.
[2] Kramer U. Metal, Hyperaccumulation in plants, Annu. Rev. Plant Biol. 61 (2010) 517–534.
[3] N.S. Pence, P.B. Larsen, S.D. Ebbs, D.L.D. Letham, M.M. Lasat, D.F. Garvin, D. Eide, L.V. Kochian, The molecular physiology of heavy metal transport in the Zn/Cd hyperaccumulator *Thlaspi caerulescens*, Proc. Natl. Acad. Sci. U. S. A. 97 (2000) 4956–4960.
[4] N.H. Roosens, C. Bernard, R. Leplae, N. Verbruggen, Evidence for copper homeostasis function metallothionein of metallothionein (MT3) in the hyperaccumulator *Thlaspi caerulescens*, FEBS Lett. 577 (2004) 9–16.
[5] J.P. Hammond, H.C. Bowen, P.J. White, V. Mills, K.A. Pyke, A.J. Baker, S.N. Whiting, S.T. May, M.R. Broadley, A comparison of the *Thlaspi caerulescens* and *Thlaspi arvense* shoot transcriptomes, New Phytol. 170 (2006) 239–260.
[6] J.E. van de Mortel, V.L. Almar, H. Schat, J. Kwekkeboom, S. Coughlan, P.D. Moerland, v.T. Ver Loren, M. Koornneef, M.G. Aarts, Large expression differences in genes for iron and zinc homeostasis, stress response, and lignin biosynthesis distinguish roots of *Arabidopsis thaliana* and the related metal hyperaccumulator *Thlaspi caerulescens*, Plant Physiol. 142 (2006) 1127–1147.
[7] J.E. van de Mortel, H. Schat, P.D. Moerland, v.T. Ver Loren, E.S. van der, H. Blankestijn, A. Ghandilyan, S. Tsiatsiani, M.G. Aarts, Expression differences for genes involved in lignin, glutathione and sulphate metabolism in response to cadmium in *Arabidopsis thaliana* and the related Zn/Cd-hyperaccumulator *Thlaspi caerulescens*, Plant Cell Environ. 31 (2008) 301–324.
[8] M. Margoshes, B.L. Vallee, A cadmium protein from equine kidney cortex, J. Am. Chem. Soc. 79 (2002) 4813–4814.
[9] P.A. Binz, J.H. Kägi, Metallothionein: molecular evolution and classification, in: C.D. Klaassen (Ed.), Metallothionein IV, Birkhauser Verlag, Basel, 1999, pp. 7–13.
[10] E. Freisinger, Structural features specific to plant metallothioneins, J. Biol. Inorg. Chem. 16 (2011) 1035–1045.
[11] W.F. Furey, A.H. Robbins, L.L. Clancy, D.R. Winge, B.C. Wang, C.D. Stout, Crystal structure of Cd, Zn metallothionein, Experientia Suppl. 52 (1987) 139–148.
[12] J.D. Otvos, R.W. Olafson, I.M. Armitage, Structure of an invertebrate metallothionein from *Scylla serrata*, J. Biol. Chem. 257 (1982) 2427–2431.
[13] R. Riek, B. Precheur, Y. Wang, E.A. Mackay, G. Wider, P. Guntert, A. Liu, J.H. Kagi, K. Wüthrich, NMR structure of the sea urchin (*Strongylocentrotus purpuratus*) metallothionein MTA, J. Mol. Biol. 291 (1999) 417–428.
[14] E.A. Peroza, R. Schmucki, P. Guntert, E. Freisinger, O. Zerbe, The beta(E)-domain of wheat E(c)-1 metallothionein: a metal-binding domain with a distinctive structure, J. Mol. Biol. 387 (2009) 207–218.
[15] J. Loebus, E.A. Peroza, N. Bluthgen, T. Fox, W. Meyer-Klaucke, O. Zerbe, E. Freisinger, Protein and metal cluster structure of the wheat metallothionein domain gamma-E(c)-1: the second part of the puzzle, J. Biol. Inorg. Chem. 16 (2011) 683–694.
[16] K. Bilecen, U.H. Ozturk, A.D. Duru, T. Sutlu, M.V. Petoukhov, D.I. Svergun, M.H. Koch, U.O. Sezerman, I. Cakmak, Z. Sayers, *Triticum durum* metallothionein. Isolation of the gene and structural characterization of the protein using solution scattering and molecular modeling, J. Biol. Chem. 280 (2005) 13701–13711.
[17] M.E. Merrifield, J. Chaseley, P. Kille, M.J. Stillman, Determination of the Cd/S cluster stoichiometry in *Fucus vesiculosus* metallothionein, Chem. Res. Toxicol. 19 (2006) 365–375.
[18] J. Domenech, R. Orihuela, G. Mir, M. Molinas, S. Atrian, M. Capdevila, The Cd(II)-binding abilities of recombinant *Quercus suber* metallothionein: bridging the gap between phytochelatins and metallothioneins, J. Biol. Inorg. Chem. 12 (2007) 867–882.
[19] J. Domenech, A. Tinti, M. Capdevila, S. Atrian, A. Torreggiani, Structural study of the zinc and cadmium complexes of a type 2 plant (*Quercus suber*) metallothionein: insights by vibrational spectroscopy, Biopolymers 86 (2007) 240–248.
[20] E.A. Peroza, E. Freisinger, Metal ion binding properties of *Triticum aestivum* Ec-1 metallothionein: evidence supporting two separate metal thiolate clusters, J. Biol. Inorg. Chem. 12 (2007) 377–391.
[21] C. Bernard, N. Roosens, P. Czernic, M. Lebrun, N. Verbruggen, A novel CPx-ATPase from the cadmium hyperaccumulator *Thlaspi caerulescens*, FEBS Lett. 569 (2004) 140–148.
[22] N.H. Roosens, R. Leplae, C. Bernard, N. Verbruggen, Variations in plant metallothioneins: the heavy metal hyperaccumulator *Thlaspi caerulescens* as a study case, Planta 222 (2005) 716–729.
[23] H. Zhong, S.L. Marcus, L. Li, Microwave-assisted acid hydrolysis of proteins combined with liquid chromatography MALDI MS/MS for protein identification, J. Am. Soc. Mass Spectrom. 16 (2005) 471–481.
[24] U.P. Fringeli, H.H. Günthard, Infrared membrane spectroscopy, Mol. Biol. Biochem. Biophys. 31 (1981) 270–332.
[25] V. Raussens, J.M. Ruysschaert, E. Goormaghtigh, Analysis of $^{1}H/^{2}H$ exchange kinetics using model infrared spectra, Appl. Spectrosc. 58 (2004) 68–82.
[26] E. Goormaghtigh, J.M. Ruysschaert, Subtraction of atmospheric water contribution in Fourier transform infrared spectroscopy of biological membranes and proteins, Spectrochim. Acta 50A (1994) 2137–2144.
[27] E. Goormaghtigh, L. Vigneron, G.A. Scarborough, J.M. Ruysschaert, Tertiary conformational changes of the *Neurospora crassa* plasma membrane H^{+}-ATPase monitored by hydrogen/deuterium exchange kinetics. A Fourier transformed infrared spectroscopy approach, J. Biol. Chem. 269 (1994) 27409–27413.
[28] V. Raussens, V. Narayanaswami, E. Goormaghtigh, R.O. Ryan, J.M. Ruysschaert, Hydrogen/deuterium exchange kinetics of apolipophorin-III in lipid-free and phospholipid-bound states. An analysis by Fourier transform infrared spectroscopy, J. Biol. Chem. 271 (1996) 23089–23095.
[29] V. Grimard, C. Vigano, A. Margolles, R. Wattiez, H.W. van-Veen, W.N. Konings, J.M. Ruysschaert, E. Goormaghtigh, Structure and dynamics of the membrane-embedded domain of LmrA investigated by coupling polarized ATR-FTIR spectroscopy and $^{1}H/^{2}H$ exchange, Biochemistry 40 (2001) 11876–11886.
[30] M. Voue, E. Goormaghtigh, F. Homble, J. Marchand-Brynaert, J. Conti, S. Devouge, J. De Coninck, Biochemical interaction analysis on ATR devices: a wet chemistry approach for surface functionalization, Langmuir 23 (2007) 949–955.
[31] S. Devouge, J. Conti, A. Goldsztein, E. Gosselin, A. Brans, M. Voue, J. De Coninck, F. Homble, E. Goormaghtigh, J. Marchand-Brynaert, Surface functionalization of germanium ATR devices for use in FTIR-biosensors, J. Colloid Interface Sci. 332 (2009) 408–415.
[32] V. Raussens, M. Pezolet, J.M. Ruysschaert, E. Goormaghtigh, Structural difference in the H^{+}, K^{+}-ATPase between the E1 and E2 conformations an attenuated total reflection infrared spectroscopy, UV circular dichroism and Raman spectroscopy study, Eur. J. Biochem. 262 (1999) 176–183.
[33] V. Raussens, J.M. Ruysschaert, E. Goormaghtigh, Protein concentration is not an absolute prerequisite for the determination of secondary structure from circular dichroism spectra: a new scaling method, Anal. Biochem. 319 (2003) 114–121.
[34] T. Gan, A. Munoz, C.F. Shaw III, D.H. Petering, Reaction of 111Cd7-metallothionein with EDTA. A reappraisal, J. Biol. Chem. 270 (1995) 5339–5345.
[35] S. Krimm, J. Bandekar, Vibrational spectroscopy and conformation of peptides, polypeptides, and proteins, Adv. Protein Chem. 38 (1986) 181–364.
[36] E. Goormaghtigh, V. Cabiaux, J.M. Ruysschaert, Determination of soluble and membrane protein structure by Fourier transform infrared spectroscopy. III. Secondary structures, subcell, Biochemistry 23 (1994) 405–450.
[37] E. Goormaghtigh, V. Cabiaux, J.M. Ruysschaert, Determination of soluble and membrane protein structure by Fourier transform infrared spectroscopy. I. Assignments and model compounds, subcell, Biochemistry 23 (1994) 329–362.
[38] A. Barth, C. Zscherp, What vibrations tell us about proteins, Q. Rev. Biophys. 35 (2002) 369–430.
[39] N.N. Kalnin, I.A. Baikalov, S.Y. Venyaminov, Quantitative IR spectrophotometry of peptide compounds in water (H_2O) solutions. III. Estimation of the protein secondary structure, Biopolymers 30 (1990) 1273–1280.

[40] E. Goormaghtigh, J.M. Ruysschaert, V. Raussens, Evaluation of the information content in infrared spectra for protein secondary structure determination, Biophys. J. 90 (2006) 2946–2957.
[41] K.A. Oberg, J.M. Ruysschaert, E. Goormaghtigh, Rationally selected basis proteins: a new approach to selecting proteins for spectroscopic secondary structure analysis, Prot. Sci. 12 (2003) 2015–2031.
[42] C.A. Orengo, A.D. Michie, S. Jones, D.T. Jones, M.B. Swindells, J.M. Thornton, CATH—a hierarchic classification of protein domain structures, Structure 5 (1997) 1093–1108.
[43] A. Torreggiani, J. Domènech, R. Orihuela, C. Ferreri, S. Atrian, M. Capdevila, C. Chatgilialoglu, Zinc and cadmium complexes of a plant metallothionein under radical stress: desulfurisation reactions associated with the formation of trans-lipids in model membranes, Chemistry 15 (2009) 6015–6024.
[44] A. Torreggiani, J. Domenech, S. Atrian, M. Capdevila, A. Tinti, Raman study of in vivo synthesized Zn(II)-metallothionein complexes: structural insight into metal clusters and protein folding, Biopolymers 89 (2008) 1114–1124.
[45] C. Vigano, J.M. Ruyssehaert, E. Goormaghtigh, Sensor applications of attenuated total reflection infrared spectroscopy, Talanta 65 (2005) 1132–1142.
[46] F. Scheirlinckx, V. Raussens, J.M. Ruysschaert, E. Goormaghtigh, Conformational changes in gastric H^+/K^+-ATPase monitored by difference Fourier-transform infrared spectroscopy and hydrogen/deuterium exchange, Biochem. J. 382 (2004) 121–129.
[47] R.B. Gregory, R. Lumry, Hydrogen-exchange evidence for distinct structural classes in globular proteins, Biopolymers 24 (1985) 301–326.
[48] D.G. Knox, A. Rosenberg, Fluctuations of protein structure as expressed in the distribution of hydrogen exchange rate constants, Biopolymers 19 (1980) 1049–1068.
[49] S.W. Provencher, V.G. Dovi, Direct analysis of continuous relaxation spectra, J. Biochem. Biophys. Methods 1 (1979) 313–318.
[50] H.H. de-Jongh, E. Goormaghtigh, J.M. Ruysschaert, Amide-proton exchange of water-soluble proteins of different structural classes studied at the submolecular level by infrared spectroscopy, Biochemistry 36 (1997) 13603–13610.
[51] Alegre-CebolladaJ. , A.M. del Pozo, J.G. Gavilanes, E. Goormaghtigh, Infrared spectroscopy study on the conformational changes leading to pore formation of the toxin sticholysin II, Biophys. J. 93 (2007) 3191–3201.
[52] V. Grimard, C.H. Li, M. Ramjeesingh, C.E. Bear, E. Goormaghtigh, J.M. Ruysschaert, Phosphorylation-induced conformational changes of cystic fibrosis transmembrane conductance regulator monitored by attenuated total reflection-Fourier transform IR spectroscopy and fluorescence spectroscopy, J. Biol. Chem. 279 (2004) 5528–5536.
[53] N. Sonveaux, A.B. Shapiro, E. Goormaghtigh, V. Ling, J.M. Ruysschaert, Secondary and tertiary structure changes of reconstituted P-glycoprotein. A Fourier transform attenuated total reflection infrared spectroscopy analysis, J. Biol. Chem. 271 (1996) 24617–24624.
[54] A. Barth, The infrared absorption of amino acid side chains, Prog. Biophys. Mol. Biol. 74 (2000) 141–173.
[55] E. Goormaghtigh, V. Cabiaux, J.M. Ruysschaert, Determination of soluble and membrane protein structure by Fourier transform infrared spectroscopy. II. Experimental aspects, side chain structure, and H/D exchange, Subcell. Biochem. 23 (1994) 363–403.
[56] N. Dave, V.A. Lorenz-Fonfria, J. Villaverde, R. Lemonnier, G. Leblanc, E. Padros, Study of amide-proton exchange of *Escherichia coli* melibiose permease by attenuated total reflection-Fourier transform infrared spectroscopy: evidence of structure modulation by substrate binding, J. Biol. Chem. 277 (2002) 3380–3387.
[57] T.N. Earnest, J. Herzfeld, K.J. Rothschild, Polarized Fourier transform infrared spectroscopy of bacteriorhodopsin. Transmembrane alpha helices are resistant to hydrogen/deuterium exchange, Biophys. J. 58 (1990) 1539–1546.
[58] N. Methot, C.N. Demers, J.E. Baenziger, Structure of both the ligand- and lipid-dependent channel-inactive states of the nicotinic acetylcholine receptor probed by FTIR spectroscopy and hydrogen exchange, Biochemistry 34 (1995) 15142–15149.
[59] P. Rath, W.J. DeGrip, K.J. Rothschild, Photoactivation of rhodopsin causes an increased hydrogen-deuterium exchange of buried peptide groups, Biophys. J. 74 (1998) 192–198.
[60] Y.P. Zhang, R.N. Lewis, R.S. Hodges, R.N. McElhaney, FTIR spectroscopic studies of the conformation and amide hydrogen exchange of a peptide model of the hydrophobic transmembrane alpha-helices of membrane proteins, Biochemistry 31 (1992) 11572–11578.
[61] E. Freisinger, Spectroscopic characterization of a fruit-specific metallothionein: *M. acuminata* MT3, Inorg. Chim. Acta 360 (2007) 369–380.
[62] S.N.A. Abdullah, S.C. Cheah, D.J. Murphy, Isolation and characterisation of two divergent type 3 metallothioneins from oil palm, *Elaeis guineensis*, Plant Physiol. Biochem. 40 (2002) 255–263.
[63] W. Bernhard, M. Good, M. Vasak, J.H.R. Kagi, Spectroscopic studies and characterization of metallothioneins containing mercury, lead and bismuth, Inorg. Chim. Acta 79 (1983) 154–155.
[64] J.H.R. Kagi, H.-J. Hapke, Biochemical interactions of mercury, cadmium and lead, in: J.O. Nriagu (Ed.), Changing metal cycles and human health, Springer-Verlag, Berlin, 1984, pp. 237–250.
[65] O.I. Leszczyszyn, R. Schmid, C.A. Blindauer, Toward a property/function relationship for metallothioneins: histidine coordination and unusual cluster composition in a zinc-metallothionein from plants, Proteins — Struct. Funct. Bioinf. 68 (2007) 922–935.
[66] V.H. Hassinen, M. Tuomainen, S. Peraniemi, H. Schat, S.O. Karenlampi, A.I. Tervahauta, Metallothioneins 2 and 3 contribute to the metal-adapted phenotype but are not directly linked to Zn accumulation in the metal hyperaccumulator, *Thlaspi caerulescens*, J. Exp. Bot. 60 (2009) 187–196.
[67] O. Schicht, E. Freisinger, Spectroscopic characterization of *Cicer arietinum* metallothionein 1, Inorg. Chim. Acta 362 (2009) 714–724.
[68] S. Navea, R. Tauler, E. Goormaghtigh, A. de Juan, Chemometric tools for classification and elucidation of protein secondary structure from infrared and circular dichroism spectroscopic measurements, Proteins — Struct. Funct. Bioinf. 63 (2006) 527–541.
[69] K.A. Oberg, J.M. Ruysschaert, E. Goormaghtigh, The optimization of protein secondary structure determination with infrared and CD spectra, Eur. J. Biochem. 271 (2004) 2937–2948.